Research Article

Pulmonary Circulation

Pressure overload induced right ventricular remodeling is not attenuated by the anti-fibrotic agent pirfenidone

Stine Andersen[1], Julie Birkmose Axelsen[1], Steffen Ringgaard[2], Jens Randel Nyengaard[3], Signe Holm Nielsen[4,5], Federica Genovese[4], Morten Asser Karsdal[4], Janus Adler Hyldebrandt[6], Charlotte Brandt Sørensen[1,7], Frances S. de Man[8], Harm Jan Bogaard[8], Jens Erik Nielsen-Kudsk[1] and Asger Andersen[1]

[1]Department of Cardiology, Aarhus University Hospital, Denmark; [2]MR Centre, Aarhus University Hospital, Denmark; [3]Core Center for Molecular Morphology, Section for Stereology and Microscopy, Department of Clinical Medicine; Centre for Stochastic Geometry and Advanced Bioimaging, Aarhus University, Denmark; [4]Fibrosis Biology and Biomarkers Research, Nordic Bioscience A/S, Herlev, Denmark; [5]Deparment of Biomedicine and Biotechnology, Technical University of Denmark, Lyngby, Denmark; [6]Department of Anesthesiology and Intensive Care, Aarhus University Hospital, Denmark; [7]Department of Clinical Medicine, Aarhus University, Denmark; [8]Department of Pulmonology, Amsterdam UMC, The Netherlands

Abstract

Cardiac fibrosis contributes to the development of heart failure in pulmonary hypertension. We aimed to assess the development of fibrosis and the effects of treatment with the anti-fibrotic agent pirfenidone in pressure overload induced right ventricular (RV) failure. Wistar rat weanlings were randomized to pulmonary trunk banding (PTB) or sham surgery. One week after the procedure, PTB rats were randomized into two groups with either six weeks on standard chow or treatment with pirfenidone mixed in chow (700 mg/kg/day). RV hemodynamic effects were evaluated by echocardiography, cardiac magnetic resonance imaging (MRI), and pressure-volume measurements. Sections from the isolated RV, left ventricle, and septum were sampled systematically; stereological point grids and the nucleator were used to estimate volume of fibrosis and cardiac hypertrophy, respectively. PTB caused RV failure in all rats subjected to the procedure. The volume fraction of fibrosis in the RV increased threefold in PTB rats corresponding to a sixfold increase in total volume of RV fibrosis. Volume fraction of fibrosis and total volume of fibrosis also increased in the septum and in the left ventricle. Pirfenidone reduced body weight but did not improve RV hemodynamics or reduce cardiac fibrosis. RV cardiomyocyte profile area was increased twofold in PTB rats without any effect of pirfenidone. RV pressure overload after PTB induced not only RV but also septal and left ventricular fibrosis assessed by stereology. Treatment with pirfenidone reduced body weight but did not reduce the development of cardiac fibrosis or delay the progression of RV failure.

Keywords

right ventricular function and dysfunction, remodeling, animal models

Date received: 29 January 2019; accepted: 15 April 2019

Pulmonary Circulation 2019; 9(2) 1–13
DOI: 10.1177/2045894019848659

Right ventricular (RV) failure is the predominant cause of death in pulmonary hypertension (PH) and congenital heart disease patients.[1,2] In these patients, the RV is subjected to a pathophysiological pressure overload, which may be caused by several mechanisms including pulmonary vaso-obliteration (idiopathic pulmonary arterial hypertension [IPAH]), mechanical obstruction of the pulmonary circulation (chronic thromboembolic pulmonary hypertension [CTEPH]), or congenital/post-surgical anatomical cardiac abnormalities (e.g. RV outflow tract obstruction or systemic RV). In these disorders, cardiomyocyte hypertrophy and

Corresponding author:
Stine Andersen, Department of Cardiology, Aarhus University Hospital, Palle Juul-Jensens Boulevard 99, 8200 Aarhus N, Denmark.
Email: stineandersen@clin.au.dk

interstitial changes including fibrosis dominate the RV myocardium. Excessive collagen formation and structural alterations to the collagen network of the extracellular matrix (ECM) disrupt the normal architecture of the myocardial tissue contributing to the progression of ventricular dysfunction and eventually failure. Cardiac fibrosis is associated with a stiffer ventricle and thereby impaired diastolic function, but it also disrupts the coordination of myocardial contraction and hence impairs systolic function. Furthermore, fibrotic remodeling promotes ventricular dilatation.[3] Cardiac fibrosis correlates with RV dysfunction[4,5] and predicts clinical worsening[6] in PH patients, although it is not associated with additional mortality risk.[7]

Transforming growth factor-β (TGF-β) plays a key role in the development of fibrosis and stimulates activation and proliferation of cardiac fibroblasts. In addition, TGF-β acts directly on the cardiomyocytes promoting ventricular hypertrophy and dysfunction.[8]

In experimental pressure overload induced RV failure, TGF-β and its downstream signaling pathway are upregulated;[9,10] and inhibition of TGF-β signaling reduced RV hypertrophy and pressure and improved RV function in the monocrotaline (MCT) model of PH.[11–13] A TGF-β1/3 selective ligand trap consisting of the extracellular domain of the TGF-β type 2 receptor expressed as an immunoglobulin–Fc fusion protein binding the TGF-β subtypes 1 and 3 attenuated RV fibrosis and improved RV function in the Sugen-hypoxia model of PH.[14]

Pirfenidone is used for the treatment of idiopathic pulmonary fibrosis (IPF), but its anti-fibrotic effects apply to a broad range of organs.[15] It primarily works through inhibition of TGF-β, but its exact mechanisms of action are not well understood. In addition to its anti-fibrotic effects, pirfenidone has functional effects on the cardiomyocytes through stimulation of L-type voltage-gated Ca^{++} channels;[16] and in a mice model of Duchennes muscular dystrophy, Pirfenidone improved cardiac contractility by enhancing the excitation-contraction coupling.[17] The ability of pirfenidone to reduce myocardial fibrosis has been demonstrated in a number of studies, although only the left ventricle (LV) was evaluated.[18–21] In recent studies, treatment with pirfenidone reduced pulmonary vascular remodeling and RV fibrosis in the Sugen-hypoxia model of PH[22] and RV fibrosis in pulmonary artery banded mice.[23] A phase II study investigating safety and efficacy of pirfenidone in heart failure patients with preserved ejection fraction (EF), who often present with concomitant RV dysfunction, is ongoing (NCT02932566).

Currently, no targeted RV failure treatment strategy exists despite the poor prognosis associated with the development of RV failure in a number of cardiopulmonary disorders. Treatments targeting the development of cardiac fibrosis may prevent deterioration of RV function but have only been sparsely investigated. This study was designed to evaluate the development of fibrosis and the effects of treatment with pirfenidone in pressure overload induced RV failure using stereology for a design-unbiased assessment of structural changes of the myocardium.

Methods

Study design

Rats were randomized to RV failure by pulmonary trunk banding (PTB) or to sham surgery (Sham, n = 12). One week after the procedure, echocardiography was performed to confirm the development of RV dysfunction and PTB rats were randomized to standard chow (PTB, n = 13) or pirfenidone treatment (PTB + pirf, n = 10) as 0.8% mixture in chow. To assess food intake, rats and chow from each cage were weighed twice a week. After six weeks of treatment, effects were evaluated by echocardiography, magnetic resonance imaging (MRI), and invasive pressure-volume measurements, rats were euthanized, and cardiac tissue stored for stereological evaluation of fibrosis and molecular analyses. Serum was drawn at termination and stored at $-80^{\circ}C$ for biomarker analysis

Animals and ethical approval

Male Wistar rats (Janiver Labs, France) were housed in a room with a 12-h light/dark cycle and a temperature of $23^{\circ}C$ with free access to tap water and standard rat chow (Altromin #1324; Altromin, Lage, Germany). Rats treated with pirfenidone had free access to specially made Altromin with 0.8% pirfenidone (Brogaarden, Lynge, Denmark) during the treatment period. The rats were treated according to Danish national guidelines; all experiments were approved by the Institutional Ethics Review Board and conducted in accordance with the Danish law for animal research (authorization no. 2012-15-2934-00384, Danish Ministry of Justice).

Pulmonary trunk banding

Banding of the pulmonary trunk was performed as described previously.[24] Briefly, male Wistar rat weanlings (122 ± 13 g) were anesthetized, intubated, and put on a ventilator. A lateral thoracotomy was made in order to identify and carefully separate the pulmonary trunk from the ascending aorta. A titanium clip was then compressed around the pulmonary trunk to an exact inner diameter of 0.6 mm with a modified ligating clip applier and the thorax was closed. Buprenorphine was administered subcutaneously (0.12 mg/kg) before surgery and in drinking water (7.4 mg/mL) for the following three days to relieve postoperative pain. Sham animals were subjected to the same procedure except for the application of the clip.

Hemodynamic evaluation and euthanasia

Hemodynamic effects of the PTB model and pirfenidone treatment were evaluated by echocardiography, cardiac

MRI, and invasive pressure-volume measurements. For details, see supplementary material. In short, a Vevo 2100 echocardiographic system (Visual Sonics, Canada) was used to estimate RV function. Tricuspid regurgitation was assessed in the four-chamber view using color Doppler. A 9.4-T Agilent MRI system was used to assess RV and LV volumes and cardiac output at end of study. RV and LV end-diastolic and end-systolic volumes were measured by outlining of the endocardium on a series of short-axis images through a whole heart cycle. Cardiac output was calculated from flow values from the pulmonary artery obtained by a phase contrast sequence. Before euthanasia, systemic blood pressure and RV pressures were measured invasively by two catheters (SPR-869, Millar Instruments, Houston, TX, USA) installed in the left carotid artery and the RV, respectively. Consecutive RV pressure-volume loops with decreasing preloads were obtained during slow occlusion of the inferior vena cava. Data were recorded and analyzed using LabChart software (AD Instruments, UK). For all hemodynamic measurements, analyses were performed with the observer blinded to the source of the sample.

During anesthesia, animals were euthanized by exsanguination. The heart was quickly excised and the RV and LV plus septum were separated and weighed. Signs of backward failure including ascites, hydrothorax, and liver congestion indicating decompensated RV failure were assessed.

Stereology

A stereological work flow was used for sampling and analyses of myocardial fibrosis. For details, see supplementary material. In short, the RV was cut into 2-mm slaps transverse to the apex-basis axis after 24 h fixation in formalin. The slaps were embedded in paraffin with the apical cutting face facing the surface of the paraffin block. The most apical slab with no apical cutting face was excluded. Sections of 2 μm were stained with Masson's Trichrome. Analyses were performed using an Olympus light microscope and Visiopharm software (Hørsholm, Denmark) with the observer blinded to the source of the sample. The volume fraction of fibrosis was estimated using two point grids: a 12×12 point grid for fibrosis; and a 4×4 point grid for the RV, the LV, and the septum. Interstitial, epicardial, and endocardial fibrosis were counted separately.

Volume fraction of RV fibrosis, $V_V(fib/RV)$, was calculated for each animal by the equation:

$$V_V(fib/RV) = \frac{\Sigma P(fib)}{\Sigma P(RV)} \times \frac{16}{144}$$

Reference volume of the RV, $V(RV)$, was estimated by dividing the wet weight of the RV by 1.06 (g/cm^3).[25] The total volume of RV fibrosis, $V(fib, RV)$, was then calculated as:

$$V(fib, RV) = V_V(fib/RV) \times V(RV)$$

The reference volumes of the LV and septum were estimated similarly, and the volumes of LV and septal fibrosis calculated in the same way as for the RV.

Cardiomyocyte hypertrophy was estimated for the RV, the LV, and the septum using a two-dimensional (2D) IUR nucleator probe. An unbiased counting frame was used to sample cross-sectional and longitudinal cut cardiomyocytes with a characteristic nucleus. Per rat, approximately 50 RV, 50 LV, and 50 septal cardiomyocyte profiles were measured and the averages used as representative values.

Gene expression

Messenger RNA (mRNA) was isolated from paraffin embedded RV tissue using an RNA purification kit (miRNeasy, Qiagen). Total mRNA was reverse-transcribed into complimentary DNA (cDNA) following a standard protocol and RT-qPCR were performed along with specific primers for the following genes: atrial natriuretic peptide (ANP); brain natriuretic peptide (BNP); β-myosin heavy chain (β-MHC); α-smooth muscle actin (α-SMA); TGF-β receptor 2; galectin-3 (Gal-3); Forkhead box subfamily O type 1 (FoxO1); collagen type I; collagen type III; and collagen type IV. All measured transcript expression levels were normalized to the housekeeping gene GAPDH and made relative to the normalized mRNA level of sham rats (supplementary material).

Biomarker measurements by enzyme-linked immunosorbent assay (ELISA)

The biomarkers C3M (matrix metalloproteinase [MMP]-9 mediated degradation of collagen type III), PRO-C3 (released propeptide of collagen type III, generated by a disintegrin and metalloproteinase with thrombospondin motifs-2 [ADAMTS-2], reflecting collagen type III formation), C4M (MMP-2, -9 and -12 mediated degradation of collagen type IV), and α-SMA (acetylated N-terminal of α-smooth muscle actin) were measured by competitive ELISAs developed by Nordic Bioscience (Herlev, Denmark). The biomarkers were developed and technically validated previously. Details for the individual markers can be found in supplementary material.

Statistics

Data were tested for normal distribution with the use of QQ plots. Normally distributed quantitative data are expressed as mean ± standard deviation (SD). Non-normal data were transformed and are presented as box plots. One-way analysis of variance (ANOVA) was used for evaluation of significance of differences between selected groups (PTB versus sham and PTB + pirf versus PTB), followed by post hoc Bonferroni analyses. Categorical data are presented as n (%) and Fisher's exact test was used for comparison between groups. Correlations between serum biomarker

levels and measurements of fibrosis were performed using the Spearman's correlation. All statistical analyses were performed with the use of Graphpad Prism 7 (Graphpad Software, La Jolla, CA, USA). $P < 0.05$ was considered statistically significant.

Results

PTB-induced RV failure

An echocardiography performed in all rats one week after PTB/sham operation revealed reduced RV function in PTB rats compared with sham operated rats. There was no difference in RV function between PTB rats subsequently randomized to pirfenidone treatment and PTB rats subsequently randomized to normal chow treatment (Supplemental Table S1).

At the end of the study, seven weeks after the PTB/sham operation, invasive assessment of RV pressures revealed a threefold increase in RV systolic pressure in PTB rats compared with sham rats, corresponding to a more than sixfold increase in RV afterload (arterial elastance [Ea]) (Fig. 1, Table 1). The high RV afterload caused RV systolic dysfunction evident by reduced RVEF, tricuspid annular plane systolic excursion (TAPSE), and cardiac index in PTB rats compared with sham operated rats. Increased end-systolic and end-diastolic volumes verified RV dilatation in the PTB rats (Fig. 1, Table 1). RV contractility (end-systolic elastance [Ees]) was increased in PTB rats but not enough to prevent RV-pulmonary arterial uncoupling

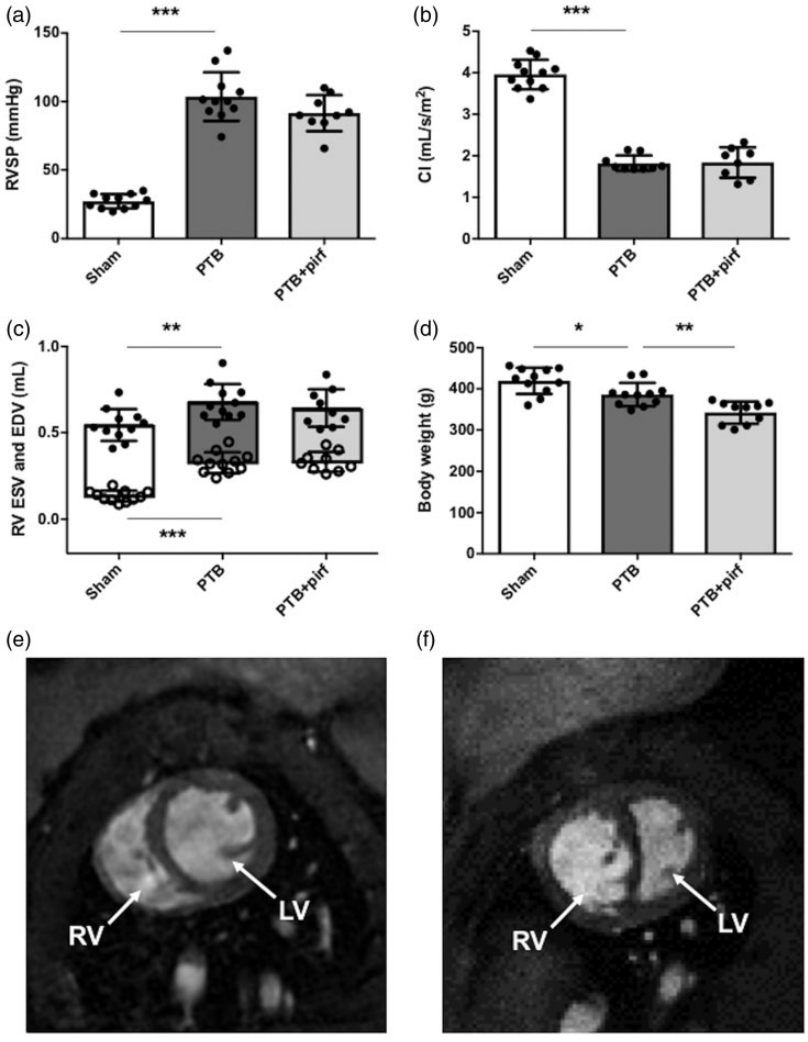

Fig. 1. Effects of PTB and pirfenidone treatment on hemodynamics and body weight. (a) At the end of the study seven weeks after PTB or sham operation, RV systolic pressure (RVSP) was increased and (b) RV cardiac index (CI) reduced in the PTB rats. (c) RV dilatation was evident by an increase in RV end-diastolic volume (EDV) and end-systolic volume (ESV) (open dots). (d) Six weeks of pirfenidone treatment lowered body weight compared with untreated rats. Representative short-axis MRI images of (e) a sham rat and (f) a PTB rat with RV hypertrophy and dilatation. Data are presented as mean ± SD. *$P < 0.05$, **$P < 0.01$, ***$P < 0.001$.

Table 1. Data at the end of the study seven weeks after PTB or sham surgery.

	Sham (n = 11)	PTB (n = 11)	PTB + pirf (n = 10)
Anatomical data			
RV weight (g)	0.22 ± 0.02	0.49 ± 0.07*	0.47 ± 0.4
LV + S weight (g)	0.86 ± 0.07	0.87 ± 0.10	0.74 ± 0.09†
RV/LV + S	0.26 ± 0.02	0.57 ± 0.09*	0.63 ± 0.04
RV/tibia length (mg/mm)	5.4 ± 0.4	12.0 ± 1.6	12.5 ± 2.8
LV + S/tibia length (mg/mm)	21.0 ± 1.2	21.3 ± 2.3	18.6 ± 2.0†
Hemodynamic measures			
Heart rate (bpm)	329 ± 19	279 ± 30*	276 ± 25
RV stroke volume (mL)	0.40 ± 0.05	0.23 ± 0.03*	0.20 ± 0.03
RV EF (%)	74 ± 4	51 ± 5*	47 ± 8
RV EDP (mmHg)	4.2 ± 3.1	8.9 ± 5.9	8.3 ± 4.6
RV filling pressure (mmHg)	1.6 ± 0.4	5.3 ± 1.8*	3.5 ± 1.0†
RV dP/dt max (mmHg/s)	1231 ± 261	4042 ± 816*	3408 ± 579
RV dP/dt min (mmHg/s)	−1117 ± 314	−3087 ± 452*	−2709 ± 585
Ea (mmHg/mL)	70 ± 19	458 ± 85*	463 ± 99
Ees (mmHg/mL)	108 ± 35	277 ± 95*	253 ± 77
Ees/Ea	1.56 ± 0.55	0.47 ± 0.17*	0.53 ± 0.15
Eed (mmHg/mL)	2.7 ± 1.2	19.2 ± 13.0§	15.8 ± 12.1
RV PRSW (mmHg)	22 ± 9	50 ± 22§	39 ± 13
TAPSE (mm)	2.5 ± 0.1	1.6 ± 0.3*	1.7 ± 0.2
LV EDV (mL)	0.64 ± 0.06	0.42 ± 0.05*	0.40 ± 0.06
LV ESV (mL)	0.16 ± 0.03	0.13 ± 0.04	0.13 ± 0.03
LV EF (%)	75 ± 5	68 ± 6‡	66 ± 6
MAP (mmHg)	109 ± 11	113 ± 8	117 ± 12

Data are presented as mean ± SD or n.
*$P < 0.001$ vs. sham.
†$P < 0.01$ vs. PTB.
‡$P < 0.05$ vs. sham.
§$P < 0.01$ vs. sham.
RV, right ventricle; LV + S, left ventricle plus septum; LV, left ventricle; EDP, end-diastolic pressure; RV dP/dt, first derivative of right ventricular systolic pressure; Ea, arterial elastance; Ees, end-systolic elastance; Eed, end-diastolic elastance; PRSW, preload recruitable stroke work; TAPSE, tricuspid annular plane systolic excursion; EDV, end-diastolic volume; ESV, end-systolic volume; EF, ejection fraction; MAP, mean arterial pressure.

(Ees/Ea). Moreover, the PTB procedure increased RV diastolic stiffness (end-diastolic elastance [Eed]) (Table 1).

In some rats, banding of the pulmonary trunk caused decompensated RV failure with signs of backward failure. In the PTB group, 6/11 rats presented with signs of liver congestion verified by a dark discoloration of the liver (nutmeg liver). Fluid retention (ascites and hydrothorax) was observed in 3/11 rats (Supplemental Table S2). None of the sham rats had signs of backward failure.

RV failure was also confirmed on the molecular level by increased gene expression of the heart failure markers ANP and BNP and the hypertrophy marker β-MHC in the PTB rats compared with sham operated rats (Fig. 2). FoxO1 gene expression level did not differ between PTB and sham operated rats.

Three rats died after randomization and before the end of the study; one sham rat and two PTB rats were randomized to normal chow. All three rats died from late respiratory complications of the surgical procedures.

PTB caused RV fibrosis and hypertrophy

RV, LV, and septal fibrosis were assessed by stereology. In the RV, the volume fraction of interstitial fibrosis increased threefold in the PTB rats compared with sham, which corresponded to a sixfold increase in absolute volume of interstitial RV fibrosis. For the septum, the banding caused a similar threefold increase in the volume fraction of interstitial fibrosis corresponding to a threefold increase in absolute volume of interstitial septal fibrosis. Likewise, the volume fraction and the absolute volume of LV interstitial fibrosis was higher in the PTB rats compared with sham operated rats (Fig. 3). Volume fraction and absolute volume of total fibrosis (interstitial fibrosis plus endo- and epicardium) were also higher in the PTB rats compared with sham for the RV, the septum, and the LV (Supplemental Table S3). Average areal shrinkage between fixed tissue and paraffin sections for all samples was 27 ± 12%, with no differences between the groups. RV hypertrophy was evident by a more than twofold increase in RV cardiomyocyte profile area. There was no difference in septal and LV cardiomyocyte profile areas between the PTB rats and the sham rats (Fig. 4).

Gene expression levels of the two primary cardiac collagen types, collagen I and collagen III, were increased in the PTB rats compared with sham operated rats, while the collagen I/collagen III ratio did not differ between the groups. Gene expression of the pro-fibrotic lectin galectin-3 was increased in the PTB rats; and an increase in the myofibroblast marker α-SMA indicated cardiac fibroblast-to-myofibroblast activation in the PTB rats (Fig. 2). Serum levels of the biomarker C3M decreased in the PTB rats compared with sham rats, while serum levels of the biomarkers PRO-C3, C4M, and α-SMA did not differ between the groups. C3M and α-SMA concentrations negatively correlated with RV interstitial fibrosis in the PTB rats, but not in the sham rats (Fig. 5).

Effects of treatment with pirfenidone

At the end of the study, seven weeks after PTB operation, rats treated with pirfenidone had a lower body weight compared to non-treated PTB rats (Fig. 1). Average daily food intake did not differ between the group receiving standard chow and the group receiving chow mixed with pirfenidone (PTB: 23.1 ± 0.1 g/day vs. PTB + pirf: 22.5 ± 0.5 g/day, $P = 0.77$). Pirfenidone treatment did not lower RV afterload or improve RV contractility. This led to an unaltered RV-pulmonary arterial coupling in the pirfenidone-treated PTB rats compared with non-treated PTB rats (Table 1). RV function was not improved by pirfenidone as TAPSE, cardiac index, and RVEF did not differ between the two PTB

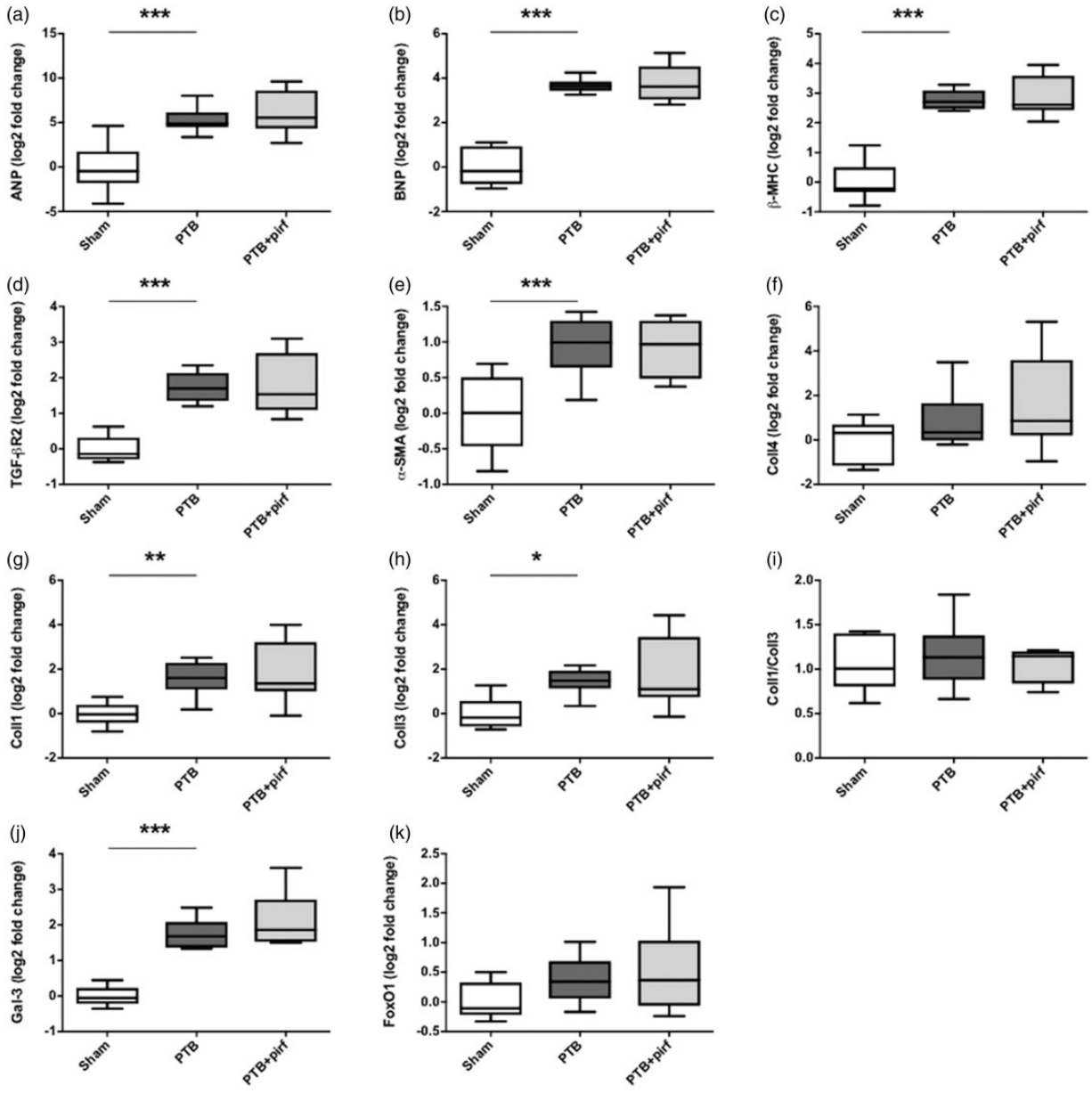

Fig. 2. Effects of PTB and pirfenidone on gene expressions. mRNA expression levels of (a) atrial natriuretic peptide (ANP), (b) brain natriuretic peptide (BNP), (c) β-myosin heavy chain (β-MHC), (d) transforming growth factor-β (TGF-β) receptor type 2, (e) α-smooth muscle actin (α-SMA), (f) collagen IV (Coll4), (g) collagen I (Coll1), (h) collagen III (Coll3), (i) the collagen I/III ratio, (j) galectin-3 (Gal-3), and (k) FoxO1. Data are presented as box plots with whiskers representing minimum and maximum values. $^{*}P < 0.05$, $^{**}P < 0.01$, $^{***}P < 0.001$.

groups. Likewise, pirfenidone treatment did not reduce RV dilatation as RV end-diastolic and end-systolic volumes were similar in the PTB and the PTB + pirf groups (Fig. 1, Table 1). There was no difference in the proportions of rats with signs of backward failure between the pirfenidone treated rats and the non-treated PTB rats (Supplemental Table S2).

Pirfenidone-treated PTB rats had lower LV + S weight and LV + S weight/tibia length ratio compared with non-treated PTB rats (Table 1). However, there was no difference in LV or septal cardiomyocyte profile area or LV + S weight/body weight ratio between the PTB + pirf and the PTB rats (Fig. 4, Supplemental Table S2). Treatment with pirfenidone did not reduce the volume fraction of interstitial fibrosis in either the RV, the septum, or the LV. Neither did the soluble biomarkers of fibrosis change after treatment. The absolute volume of interstitial fibrosis in the septum was lower in the pirfenidone-treated PTB rats compared with control PTB rats; a trend towards a similar decrease was seen in the LV ($P = 0.07$) (Fig. 3).

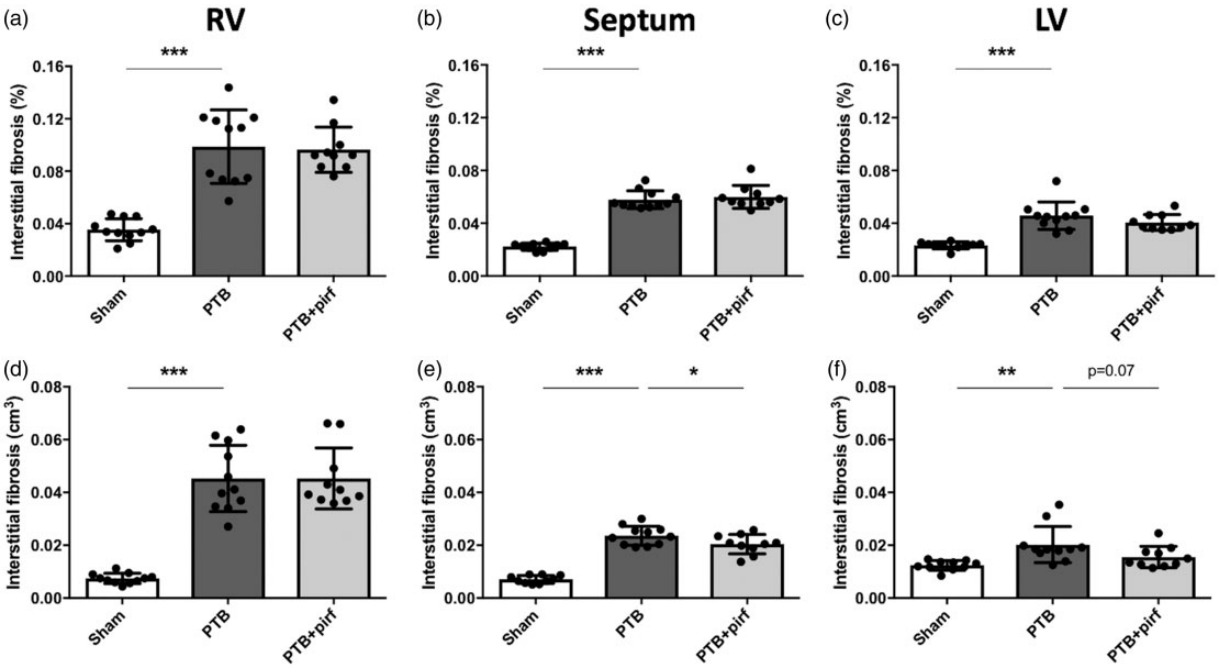

Fig. 3. Effects of PTB and pirfenidone on interstitial fibrosis. At the end of the study, volume fraction of fibrosis was increased in (a) the RV, (b) the septum, and (c) the LV of PTB rats compared with sham. (d–f) Likewise, absolute volume of fibrosis was increased. Pirfenidone-treated PTB had (e) lower absolute volumes of fibrosis in the septum and (f) a trend towards a lower volume in the LV due to the lower volumes of the septum and the LV in the PTB + pirf rats compared with PTB control rats. Data are presented as mean ± SD. $^{*}P < 0.05$, $^{**}P < 0.01$, $^{***}P < 0.001$.

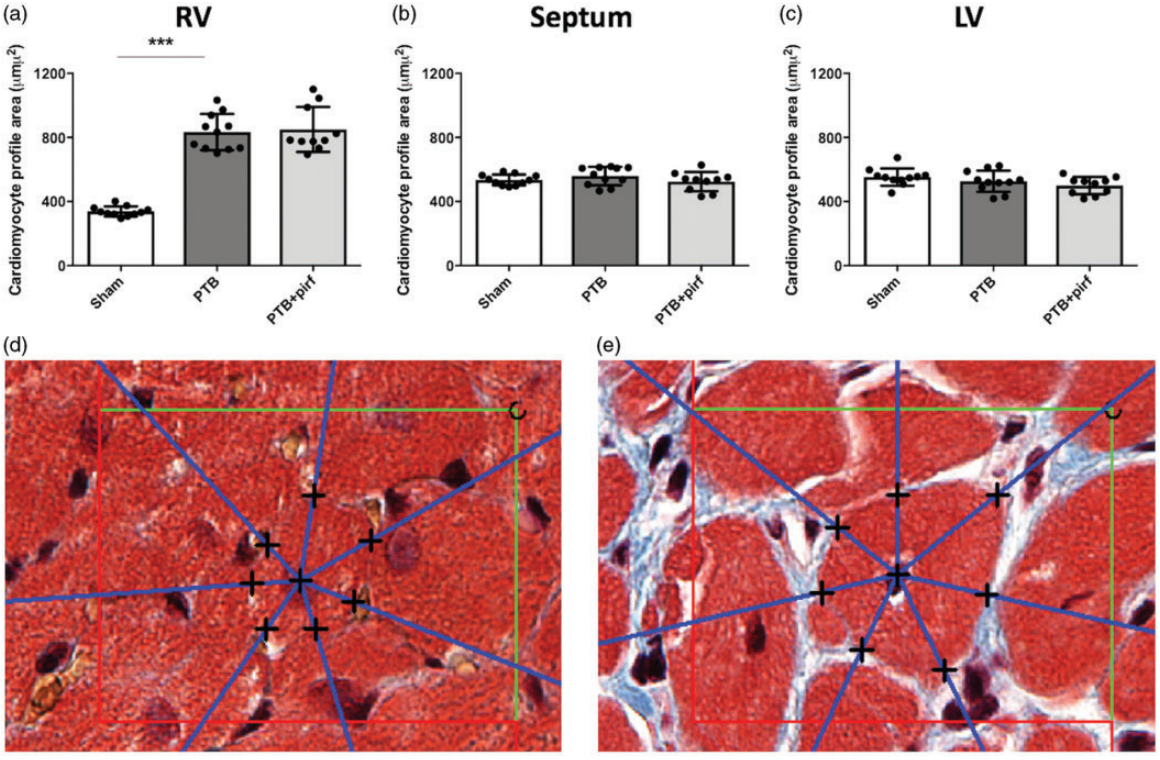

Fig. 4. Effects of PTB and pirfenidone on cardiomyocyte profile area. (a) An increase in average cardiomyocyte profile area confirmed RV hypertrophy in the PTB rats. (b, c) There was no difference in septal or LV cardiomyocyte profile areas in the PTB rats compared with sham rats. (a–c) Pirfenidone treatment had no effects on cardiomyocyte profile area in either the RV, the septum, or the LV. Representative images of RV cardiomyocytes from (d) a sham rat and (e) a PTB rat with the test rays of the 2D IUR nucleator diverging from the nucleus of the cardiomyocytes. The black crosses indicate the intersections of the half-lines with the membrane of the cardiomyocyte profiles. The area of the unbiased counting frame is 3272 μm^2. Data are presented as mean ± SD. $^{***}P < 0.001$.

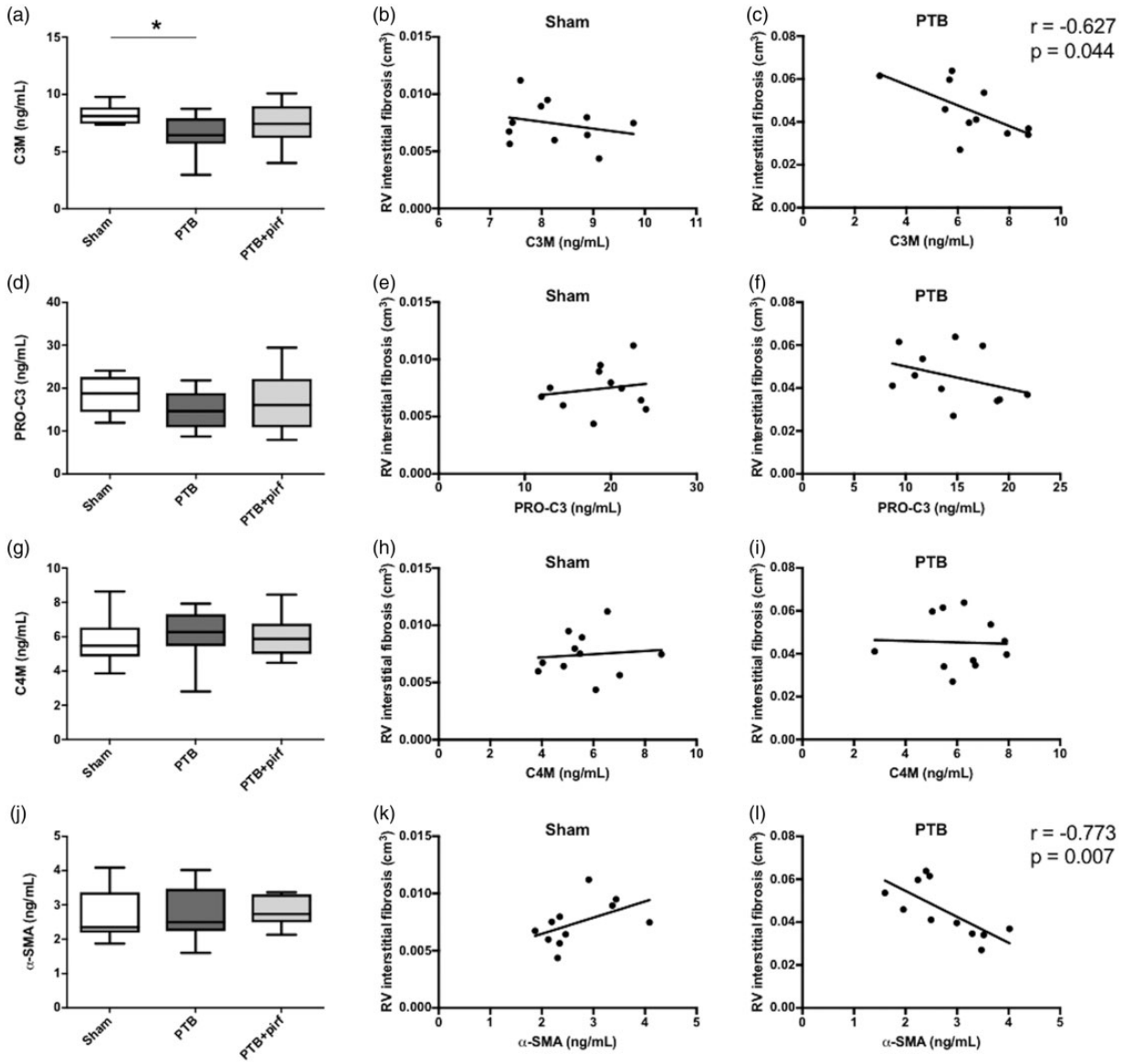

Fig. 5. Biomarkers and RV fibrosis. Serum levels of (a) C3M and the correlations between serum C3M and RV interstitial fibrosis for (b) the sham rats and (c) the PTB rats at end of study. Serum level and correlations are shown similarly for (d–f) PRO-C3, (g–i) C4M, and (j–l) α-SMA. Serum levels are presented as box plots with whiskers representing minimum and maximum values. Spearman's correlation coefficient is shown only for statistically significant correlations. *$P < 0.05$.

Discussion

Applying an extensive hemodynamic evaluation and stereological investigation in a rat model of pressure overload induced RV failure, we have demonstrated that:

- RV pressure overload after banding of the pulmonary trunk induced RV failure in all rats subjected to the procedure;
- fibrosis developed in the pressure overloaded RV and to a lesser extent in the septum and the LV of the PTB rats, while cardiomyocyte hypertrophy was characteristic only for the RV;
- treatment with the anti-fibrotic agent pirfenidone reduced body weight but did not reduce the development of cardiac fibrosis or delay the progression of RV failure.

The PTB model is a valid model of RV failure and fibrosis

The PTB procedure caused RV failure evident by a decrease in cardiac output, RV-pulmonary arterial uncoupling and extracardiac manifestations in the form of liver congestion as a result of backward failure. The PTB model used in this study is thus a model of severe RV failure.

We found a marked increase in RV fibrosis in the PTB rats, which has also been observed in other studies using different methods to band the pulmonary trunk either by partial ligation or, as in this study, by a ligating clip.[26–28] However, the severity of the banding seems critical in provoking the fibrotic response of the pressure overloaded RV, as rats subjected to a mild banding using a ligature and a 16-G needle showed only a minor and non-significant increase in RV fibrosis, while another group of rats from the same study subjected to severe banding (18-G needle) developed a marked increase in fibrosis.[28] A mild banding incapable of inducing fibrosis may also explain why not all studies observe increased fibrosis after banding of the pulmonary trunk.[29]

We found the collagen volume fraction in the healthy RV to be slightly higher than the collagen fraction in the healthy LV and septum (Supplemental Figure S2), which is in line with previous findings in rats[30] and human.[31] This interventricular difference may be explained by the relative atrophy of the RV cardiomyocytes after birth compared with the LV cardiomyocytes[32] and the different embryological origin of the two ventricles.[33] In accordance with this, RV cardiomyocytes were smaller compared with septal and LV cardiomyocytes in the sham rats of this study (Supplemental Figure S3).

Four circulating biomarkers of fibrosis, C3M, PRO-C3, C4M, and α-SMA, were measured to evaluate whether they could be used as diagnostic biomarkers or efficacy of treatment biomarkers in rats with RV failure and fibrosis. Assessment of biomarkers could not only aid translational research, but potentially be used for diagnostic, prognostic, and therapeutic decisions in clinical practice.[34–37] In this study, the only circulating biomarker able to distinguish between sham operated rats and PTB rats was C3M. This result suggests that C3M may be used as a non-invasive marker of fibrosis for this model; however, the ability of C3M to be used as an efficacy of treatment marker cannot be elucidated since pirfenidone did not work on the fibrosis in this study. C3M was negatively correlated with RV interstitial fibrosis, indicating that higher levels of C3M, a degradation fragment of collagen type III reflected a lower level of RV interstitial fibrosis. C3M is generated by MMP-2 and -9 and it has previously been shown that reduced MMP-2 activity contributes to cardiac fibrosis in rats.[38] The reduced activity of MMPs may therefore explain the reduced release of C3M fragments into circulation. Neither PRO-C3, C4M, or α-SMA showed a significant difference in the serum levels from sham, PTB, or PTB + pirf treated rats; however the levels of α-SMA in circulation was strongly correlated to RV interstitial fibrosis in the PTB-treated rats. While mRNA levels of α-SMA were upregulated, the protein levels released in serum showed the opposite trend. This could be explained by a difference in the amount of α-SMA released in circulation compared to the α-SMA deposited in the tissue.[39]

We observed an increase in TGF-β receptor type 2 gene expression in the PTB rats, which corresponds with other studies using experimental models of pressure overload induced RV failure.[9,10] In PAH patients a (non-significant) increase in TGF-β receptor 1 has been demonstrated.[40] The type 1 and type 2 TGF-β receptors are transmembrane serine/threonine kinases adhering to each other when binding the ligand TGF-β1 to phosphorylate the intracellular signaling molecules Smad2 and Smad3. Interestingly a decrease in the expression of TGF-β related genes have been observed in patients with tetralogy of Fallot.[41] The progression of RV dysfunction and failure is usually milder in congenital heart disease patients compared with PAH patients.

RV, septal, and LV fibrosis in RV failure

In addition to RV fibrosis, we also observed increased LV fibrosis and fibrosis in the interventricular septum of the PTB rats. Histological analyses of explanted hearts from end-stage PAH patients revealed an increase in RV fibrosis and a non-significant increase in LV fibrosis.[40] In non-end stage PH patients, the LV and septum have longer T1 relaxation times (an indirect measure of fibrosis obtained by cardiac MRI) compared with patients without PH.[42,43] In other experimental models of RV failure and RV fibrosis, concomitant LV fibrosis has also been observed.[10,44]

Several mechanisms may explain the development of LV and septal fibrosis in the heart subjected to RV pressure overload. First, mechanical ventricular interdependence causes structural changes to the LV during the development of pressure overload induced RV hypertrophy and failure. Due to RV-LV dys-synchrony, the septum starts to bulge into the LV cavity[45] and LV filling decreases due to reduced RV output.[46] The consequent change in LV shape and reduction in LV size may be accompanied by changes to the LV ECM including an increase in fibrosis.

Second, neurohormonal activation, including activation of the renin-angiotensin-aldosterone-system, plays a role in the development of RV failure in rats and has been demonstrated in patients with PH and RV failure.[47] Increased levels of neurohormones might affect the whole heart and not just the pressure overload RV and trigger LV remodeling in addition to RV remodeling.

Third, the ventricular insertion points where the RV hinges the septum and the LV is subjected to massive mechanical stress and stretch, when the septum shift from a static rightward convex position to a leftward bulging situation. Accordingly, substantial increases in fibrosis are observed in these hinge points in PH patients.[48]

Effects of pirfenidone

The six-week treatment with pirfenidone reduced body weight, which is in contrast to other studies investigating the effects of pirfenidone in rats using a similar

dosage.[20,49,50] However, gastrointestinal problems and weight loss are well-known side effects of pirfenidone treatment.[51]

Pirfenidone is rapidly metabolized and eliminated in humans[52] and in rats.[53] Consequently, pirfenidone was administered as a mix in chow in this study, which is a commonly used route of administration in animal studies investigating the effects of pirfenidone on the lung, heart, kidney, and liver fibrosis.[15] For this study, a concentration of 0.8% was used. A concentration of 0.4% corresponding to a daily intake of 250–300 mg/kg/day was shown to give a constant plasma concentration of approximately 2 μm/mL and reduced LV hypertrophy and fibrosis in hypertensive rats,[53] but pirfenidone concentrations of 0.4–1.2% in chow have been widely used in different rat models.[15]

In the Sugen-hypoxia model of PH and RV failure, pirfenidone (30 mg/kg/day by mouth three times a day for three weeks) reduced RV fibrosis, but whether the reduction in RV fibrosis was secondary to the reduction in pulmonary vascular resistance also observed in the study or direct effects of pirfenidone on the RV could not be concluded.[22] Our results suggest that the reduction in RV fibrosis after pirfenidone treatment in the Sugen-hypoxia model may be explained primarily by the RV afterload reduction, as we did not observe any direct effects of pirfenidone treatment on RV fibrosis in our model of isolated RV failure. The lower absolute volume of fibrosis in the septum and the trend towards lower volume of LV fibrosis in the PTB rats after pirfenidone treatment observed in this study reflect lower volumes of the septum and LV in the PTB + pirf rats compared with the non-treated PTB rats, as there was no difference in the volume fraction of fibrosis between the groups. The study by Poble et al. also demonstrated increased FoxO1 expression in lung tissue from both PAH patients and SuHx rats after pirfenidone treatment.[22] In this study, there was no effect of pirfenidone on RV FoxO1 expression, suggesting a different regulation of FoxO1 in the RV compared with the lungs.

In a recent study, pirfenidone reduced RV fibrosis but did not improve RV function in pulmonary artery banded mice. The authors focused on galectin-3, a pro-fibrotic lectin and mediator of myocardial ECM adaptation to stress, and found that reduced fibrosis was associated with reduced galectin-3 levels in both pirfenidone-treated mice and galectin-3 knockout mice.[23] Comparably, galectin-3 levels were increased in PTB rats, but we found no effects of pirfenidone treatment. This is expected, as pirfenidone did not reduce RV fibrosis or hypertrophy in the PTB rat model.

Pirfenidone reduced LV fibrosis in mice subjected to transverse aortic constriction (TAC).[18,19] TAC causes a pressure overload of the LV and induces LV dilatation. Thus, the LV of TAC mice are subjected to a mechanical stress and stretch, which differs substantially from the stress experienced by the LV of PTB rats, where the dilated RV compresses the LV. Consequently, although we observe an increase in LV fibrosis in the PTB rats, the lack of therapeutic effects of pirfenidone on LV fibrosis in this model, in contrast to for example the TAC model, may be explained by the different character of the fibrosis causing stress applied to the myocardium.

In a canine model of tachycardia-induced heart failure, pirfenidone reduced left atrial fibrosis and vulnerability to atrial fibrosis.[54] Supraventricular tachyarrhythmias including atrial fibrillation are common in patients with PAH and RV failure,[55] and pirfenidone may possess a therapeutic potential in reducing atrial fibrosis and thereby the arrhythmogenic substrate in these patients. PTB rats have demonstrated increased susceptibility to develop ventricular tachycardia,[56] but the occurrence of supraventricular tachyarrhythmias has not been investigated. In this study, we only assessed ventricular and not atrial fibrosis.

In contrast to our findings, inhibition of TGF-β signaling reduced RV hypertrophy in the MCT model.[11–13] However, these results may be influenced by afterload reduction as concomitant reductions in RV pressures and pulmonary vascular remodeling were observed in all studies. Interaction with the pathogenic mechanisms of action of monocrotaline might also play a role, as the response to TGF-β inhibition was more pronounced in the MCT model compared with the hypoxia model.[12]

Pirfenidone-treated rats had lower LV + S weight, which caused a trend towards higher RV/LV + S ratio ($P = 0.07$) compared with non-treated PTB rats (Table 1). However, as there was no difference in LV or septal cardiomyocyte profile area or in the LV + S weight/body weight ratio between the two PTB groups, this reduction in LV + S weight seems to be caused by the pirfenidone-treated PTB rats having a lower body weight than the non-treated PTB rats and not direct effects of pirfenidone on the LV or septum.

Strengths and limitations

This study has several strengths. First, we used a well-established model of RV failure using a ligating clip to constrict the pulmonary trunk.[24] A direct comparison of the efficacy of banding by a partially compressed clip versus partial ligation demonstrated superiority of the clip as a method of inducing RV failure.[27] Second, we used design-based stereology for assessment of cardiac fibrosis and hypertrophy, which provides unbiased principles for quantification.[57]

In this study, we used Wistar rats; interspecies differences between rats and humans might restrict the translation of our findings. In order to eliminate possible effects of hormonal changes and minimize the physiological variance between the rats, we only used male rats in the study. Consequently, this study does not provide information on possible intersex differences in the development of cardiac fibrosis and RV failure after PTB. All hemodynamic measures were obtained from anaesthetized rats. To minimize the effects of the anesthesia on our results, we strictly followed a

thoroughly tested protocol of anesthesia. Due to the lack of a sham group treated with pirfenidone, we cannot exclude effects of changes in body weight on RV function and remodeling. We used paraffin sections for stereology, which are characterized by significant shrinkage. We estimated areal shrinkage systematically and found no difference between the groups. We used single thin SUR sections and could therefore only estimate cardiomyocyte profile area and not cardiomyocyte volume.

In conclusion, RV failure developed consistently in all rats subjected to the PTB procedure. By a rigorous stereological approach, we have demonstrated that in addition to pronounced RV fibrosis, milder degrees of fibrosis also develop in the septum and LV of PTB rats. On the contrary, hypertrophy was confined to the cardiomyocytes of the pressure overloaded RV. Treatment with the anti-fibrotic compound pirfenidone reduced body weight but did not diminish the development of fibrosis, decrease RV hypertrophy, or improve RV function. Nor did pirfenidone demonstrate any adverse effects on the RV suggesting that it might be safe also in RV failure patients.

Acknowledgments

The authors thank Dorte W. Qualmann and Lisa Maria Røge as well as Rikke Nørregaard, Gitte Kall, and Gitte Skou, Department of Clinical Medicine, Aarhus University for their help with the sectioning of tissues and gene expression analyses, respectively. The authors also thank Helene Andersen, Core Center for Molecular Morphology, Section for Stereology and Microscopy, Department of Clinical Medicine, Aarhus University for her assistance with preparing the sections for stereological analyses.

Conflict of interest

SHN, FG, and MAK are full-time employees at Nordic Bioscience. None of the authors received fees, bonuses, or other benefits for the work described in the manuscript. FG and MAK hold stocks in Nordic Bioscience. The patents for the ELISAs used in this work are owned by Nordic Bioscience. The funder provided support in the form of salaries for authors SHN, FG, and MAK but did not have any additional role in the study design, data collection and analysis, decision to publish, or preparation of the manuscript.

Funding

SA was supported by Aarhus University, Denmark, the Danish Heart Foundation (16-R107-A6611-22969) and Grosserer Vald. Foersom og Hustru Thyra Foersom, født Ottos Fond. Centre for Stochastic Geometry and Advanced Bioimaging is supported by Villum Foundation. This work was further funded by the Danish Research Foundation and the Danish Innovation Foundation. FdM and HJB were supported by the Netherlands CardioVascular Research Initiative, the Dutch Heart Foundation, Dutch Federation of University Medical Centres, the Netherlands Organisation for Health Research and Development, and the Royal Netherlands Academy of Sciences.

ORCID iD

Asger Andersen https://orcid.org/0000-0002-9102-3130

References

1. Tonelli AR, Arelli V, Minai OA, et al. Causes and circumstances of death in pulmonary arterial hypertension. *Am J Respir Crit Care Med* 2013; 188: 365–369.
2. Vonk Noordegraaf A, Chin KM, Haddad F, et al. Pathophysiology of the right ventricle and of the pulmonary circulation in pulmonary hypertension: an update. *Eur Respir J* 2019; 53: 1801900.
3. Kong P, Christia P and Frangogiannis NG. The pathogenesis of cardiac fibrosis. *Cell Mol Life Sci* 2013; 71: 549–574.
4. Blyth KG, Groenning BA, Martin TN, et al. Contrast enhanced-cardiovascular magnetic resonance imaging in patients with pulmonary hypertension. *Eur Heart J* 2005; 26: 1993–1999.
5. Mehta BB, Auger DA, Gonzalez JA, et al. Detection of elevated right ventricular extracellular volume in pulmonary hypertension using Accelerated and Navigator-Gated Look-Locker Imaging for Cardiac T1 Estimation (ANGIE) cardiovascular magnetic resonance. *J Cardiovasc Magn Reson* 2015; 17: 110.
6. Freed BH, Gomberg-Maitland M, Chandra S, et al. Late gadolinium enhancement cardiovascular magnetic resonance predicts clinical worsening in patients with pulmonary hypertension. *J Cardiovasc Magn Reson* 2012; 14: 11.
7. Swift AJ, Rajaram S, Capener D, et al. LGE patterns in pulmonary hypertension do not impact overall mortality. *JACC Cardiovasc Imaging* 2014; 7: 1209–1217.
8. Koitabashi N, Danner T, Zaiman AL, et al. Pivotal role of cardiomyocyte TGF-beta signaling in the murine pathological response to sustained pressure overload. *J Clin Invest* 2011; 121: 2301–2312.
9. Kapur NK, Paruchuri V, Aronovitz MJ, et al. Biventricular remodeling in murine models of right ventricular pressure overload. *PLoS One* 2013; 8: e70802.
10. Friedberg MK, Cho M-Y, Li J, et al. Adverse biventricular remodeling in isolated right ventricular hypertension is mediated by increased transforming growth factor-β1 signaling and is abrogated by angiotensin receptor blockade. *Am J Respir Cell Mol Biol* 2013; 49: 1019–1028.
11. Megalou AJ, Glava C, Oikonomidis DL, et al. Transforming growth factor-beta inhibition attenuates pulmonary arterial hypertension in rats. *Int J Clin Exp Med* 2010; 3: 332–340.
12. Long L, Crosby A, Yang X, et al. Altered bone morphogenetic protein and transforming growth factor-beta signaling in rat models of pulmonary hypertension: potential for activin receptor-like kinase-5 inhibition in prevention and progression of disease. *Circulation* 2009; 119: 566–576.
13. Zaiman AL, Podowski M, Medicherla S, et al. Role of the TGF-beta/Alk5 signaling pathway in monocrotaline-induced pulmonary hypertension. *Am J Respir Crit Care Med* 2008; 177: 896–905.
14. Yung LM, Nikolic I, Paskin-Flerlage SD, et al. A selective transforming growth factor-beta ligand trap attenuates pulmonary hypertension. *Am J Respir Crit Care Med* 2016; 194: 1140–1151.
15. Schaefer CJ, Ruhrmund DW, Pan L, et al. Antifibrotic activities of pirfenidone in animal models. *Eur Respir Rev* 2011; 20: 85–97.

16. Ramos-Mondragon R, Galindo CA, Garcia-Castaneda M, et al. Chronic potentiation of cardiac L-type Ca(2+) channels by pirfenidone. *Cardiovasc Res* 2012; 96: 244–254.
17. Van Erp C, Irwin NG and Hoey AJ. Long-term administration of pirfenidone improves cardiac function in mdx mice. *Muscle Nerve* 2006; 34: 327–334.
18. Wang Y, Wu Y, Chen J, et al. Pirfenidone attenuates cardiac fibrosis in a mouse model of TAC-induced left ventricular remodeling by suppressing NLRP3 inflammasome formation. *Cardiology* 2013; 126: 1–11.
19. Yamagami K, Oka T, Wang Q, et al. Pirfenidone exhibits cardioprotective effects by regulating myocardial fibrosis and vascular permeability in pressure-overloaded hearts. *Am J Physiol Heart Circ Physiol* 2015; 309: H512–522.
20. Nguyen DT, Ding C, Wilson E, et al. Pirfenidone mitigates left ventricular fibrosis and dysfunction after myocardial infarction and reduces arrhythmias. *Heart Rhythm* 2010; 7: 1438–1445.
21. Yamazaki T, Yamashita N, Izumi Y, et al. The antifibrotic agent pirfenidone inhibits angiotensin II-induced cardiac hypertrophy in mice. *Hypertens Res* 2011; 35: 34–40.
22. Poble PB, Phan C, Quatremare T, et al. Therapeutic effect of pirfenidone in the sugen/hypoxia rat model of severe pulmonary hypertension. *FASEB J* 2019; 33: 3670–3679.
23. Crnkovic S, Egemnazarov B, Damico R, et al. Disconnect between fibrotic response and right ventricular dysfunction. *Am J Respir Crit Care Med* 2018. Doi: 10.1164/rccm.201809-1737OC.
24. Andersen S, Schultz J, Holmboe S, et al. A pulmonary trunk banding model of pressure overload induced right ventricular hypertrophy and failure. *J Vis Exp* 2018. Doi: 10.3791/58050.
25. Bruel A, Oxlund H and Nyengaard JR. Growth hormone increases the total number of myocyte nuclei in the left ventricle of adult rats. *Growth Horm IGF Res* 2002; 12: 106–115.
26. Borgdorff MA, Bartelds B, Dickinson MG, et al. A cornerstone of heart failure treatment is not effective in experimental right ventricular failure. *Int J Cardiol* 2013; 169: 183–189.
27. Hirata M, Ousaka D, Arai S, et al. Novel model of pulmonary artery banding leading to right heart failure in rats. *Biomed Res Int* 2015; 2015: 753210.
28. Mendes-Ferreira P, Santos-Ribeiro D, Adao R, et al. Distinct right ventricle remodeling in response to pressure overload in the rat. *Am J Physiol Heart Circ Physiol* 2016; 311: H85–95.
29. Bogaard HJ, Natarajan R, Henderson SC, et al. Chronic pulmonary artery pressure elevation is insufficient to explain right heart failure. *Circulation* 2009; 120: 1951–1960.
30. Medugorac I. Collagen content in different areas of normal and hypertrophied rat myocardium. *Cardiovasc Res* 1980; 14: 551–554.
31. Oken DE and Boucek RJ. Quantitation of collagen in human myocardium. *Circ Res* 1957; 5: 357–361.
32. Caspari PG, Gibson K and Harris P. Changes in myocardial collagen in normal development and after beta blockade. *Recent Adv Stud Cardiac Struct Metab* 1975; 7: 99–104.
33. Zaffran S, Kelly RG, Meilhac SM, et al. Right ventricular myocardium derives from the anterior heart field. *Circ Res* 2004; 95: 261–268.
34. Havmoller R and Chugh SS. Plasma biomarkers for prediction of sudden cardiac death: another piece of the risk stratification puzzle? *Circ Arrhythm Electrophysiol* 2012; 5: 237–243.
35. Lopez B, Gonzalez A, Ravassa S, et al. Circulating biomarkers of myocardial fibrosis: the need for a reappraisal. *J Am Coll Cardiol* 2015; 65: 2449–2456.
36. Choi HS, Kim KH, Yoon HJ, et al. Usefulness of cardiac biomarkers in the prediction of right ventricular dysfunction before echocardiography in acute pulmonary embolism. *J Cardiol* 2012; 60: 508–513.
37. Nielsen SH, Mouton AJ, DeLeon-Pennell KY, et al. Understanding cardiac extracellular matrix remodeling to develop biomarkers of myocardial infarction outcomes. *Matrix Biol* 2019; 75–76: 43–57.
38. Van Linthout S, Seeland U, Riad A, et al. Reduced MMP-2 activity contributes to cardiac fibrosis in experimental diabetic cardiomyopathy. *Basic Res Cardiol* 2008; 103: 319–327.
39. Holm Nielsen S, Willumsen N, Leeming DJ, et al. Serological assessment of activated fibroblasts by alpha-smooth muscle actin (alpha-SMA): a noninvasive biomarker of activated fibroblasts in lung disorders. *Transl Oncol* 2018; 12: 368–374.
40. van der Bruggen CE, Happe CM, Dorfmuller P, et al. Bone morphogenetic protein receptor type 2 mutation in pulmonary arterial hypertension: a view on the right ventricle. *Circulation* 2016; 133: 1747–1760.
41. Peters TH, Sharma V, Yilmaz E, et al. DNA microarray and quantitative analysis reveal enhanced myocardial VEGF expression with stunted angiogenesis in human tetralogy of Fallot. *Cell Biochem Biophys* 2013; 67: 305–316.
42. Reiter U, Reiter G, Kovacs G, et al. Native myocardial T1 mapping in pulmonary hypertension: correlations with cardiac function and hemodynamics. *Eur Radiol* 2017; 27: 157–166.
43. Homsi R, Luetkens JA, Skowasch D, et al. Left ventricular myocardial fibrosis, atrophy, and impaired contractility in patients with pulmonary arterial hypertension and a preserved left ventricular function: a cardiac magnetic resonance study. *J Thorac Imaging* 2017; 32: 36–42.
44. Lamberts RR, Vaessen RJ, Westerhof N, et al. Right ventricular hypertrophy causes impairment of left ventricular diastolic function in the rat. *Basic Res Cardiol* 2007; 102: 19–27.
45. Palau-Caballero G, Walmsley J, Van Empel V, et al. Why septal motion is a marker of right ventricular failure in pulmonary arterial hypertension: mechanistic analysis using a computer model. *Am J Physiol Heart Circ Physiol* 2017; 312: H691–H700.
46. Marcus JT, Vonk Noordegraaf A, Roeleveld RJ, et al. Impaired left ventricular filling due to right ventricular pressure overload in primary pulmonary hypertension: noninvasive monitoring using MRI. *Chest* 2001; 119: 1761–1765.
47. de Man FS, Tu L, Handoko ML, et al. Dysregulated renin-angiotensin-aldosterone system contributes to pulmonary arterial hypertension. *Am J Respir Crit Care Med* 2012; 186: 780–789.
48. McCann GP, Gan CT, Beek AM, et al. Extent of MRI delayed enhancement of myocardial mass is related to right ventricular dysfunction in pulmonary artery hypertension. *AJR Am J Roentgenol* 2007; 188: 349–355.
49. Shimizu T, Kuroda T, Hata S, et al. Pirfenidone improves renal function and fibrosis in the post-obstructed kidney. *Kidney Int* 1998; 54: 99–109.
50. Miric G, Dallemagne C, Endre Z, et al. Reversal of cardiac and renal fibrosis by pirfenidone and spironolactone in streptozotocin-diabetic rats. *Br J Pharmacol* 2001; 133: 687–694.

51. King TE Jr, Bradford WZ, Castro-Bernardini S, et al. A phase 3 trial of pirfenidone in patients with idiopathic pulmonary fibrosis. *N Engl J Med* 2014; 370: 2083–2092.
52. Rubino CM, Bhavnani SM, Ambrose PG, et al. Effect of food and antacids on the pharmacokinetics of pirfenidone in older healthy adults. *Pulm Pharmacol Ther* 2009; 22: 279–285.
53. Mirkovic S, Seymour A-ML, Fenning A, et al. Attenuation of cardiac fibrosis by pirfenidone and amiloride in DOCA-salt hypertensive rats. *Br J Pharmacol* 2002; 135: 961–968.
54. Lee KW, Everett THt, Rahmutula D, et al. Pirfenidone prevents the development of a vulnerable substrate for atrial fibrillation in a canine model of heart failure. *Circulation* 2006; 114: 1703–1712.
55. Wanamaker B, Cascino T, McLaughlin V, et al. Atrial arrhythmias in pulmonary hypertension: pathogenesis, prognosis and management. *Arrhythm Electrophysiol Rev* 2018; 7: 43–48.
56. Schultz JG, Andersen S, Andersen A, et al. Evaluation of cardiac electrophysiological properties in an experimental model of right ventricular hypertrophy and failure. *Cardiol Young* 2015; 26: 451–458.
57. Mühlfeld C, Nyengaard JR and Mayhew TM. A review of state-of-the-art stereology for better quantitative 3D morphology in cardiac research. *Cardiovasc Pathol* 2009; 19: 65–82.